PHILOSOPHICAL TRANSACTIONS OF THE ROYAL SOCIETY A MATHEMATICAL, PHYSICAL & ENGINEERING SCIENCES

Nonlinear Waves, Patterns and Spatio-Temporal Chaos in Cellular Neural Networks

V. Perez-Munuzuri, A. P. Munuzuri, M. Gomez-Gesteira, V. Perez-Villar, L. Pivka and L. O. Chua

Phil. Trans. R. Soc. Lond. A 1995 **353**, 101-113
doi: 10.1098/rsta.1995.0093

Nonlinear waves, patterns and spatio-temporal chaos in cellular neural networks

By V. Pérez-Muñuzuri[1], A. P. Muñuzuri[1], M. Gómez-Gesteira[1], V. Pérez-Villar[1], L. Pivka[2] and L. O. Chua[2]

[1]*Group of Nonlinear Physics, Faculty of Physics, University of Santiago de Compostela, 15706 Santiago de Compostela, Spain*

[2]*Department of Electrical Engineering and Computer Sciences, University of California at Berkeley, Berkeley, CA 94720, USA*

Spatio-temporal pattern formation occurring in discretely coupled nonlinear dynamical systems has been studied numerically. In this paper, we review the possibilities of using arrays of discretely coupled nonlinear electronic circuits to study these systems. Spiral wave initiation and Turing pattern formation are some of the examples. Sidewall forcing of Turing patterns is shown to be capable of driving the system into a perfect spatial organization, namely, a rhombic pattern, where no defects occur. The dynamics of the two layers supporting Turing and Hopf modes, respectively, is analysed as a function of the coupling strength between them. The competition between these two modes is shown to increase with the diffusion between layers. As well, the coexistence of low- and high-dimensional spatio-temporal chaos is shown to occur in one-dimensional arrays.

1. Introduction

Systems of discretely coupled cells with reactions and mass, energy or electric charge transfer often serve as standard models for investigating the phenomena occurring in the transformation and transport processes in living cells, tissues, neuron networks, physiological systems and ecosystems, as well as in all forms of chemical, biochemical and biological reactors and combustion systems (Haken 1983; Glass & Mackey 1988; Murray 1989; Winfree 1987; Zykov 1987). In the continuous limit, it is possible to derive a reaction-diffusion type model which exhibits all classical properties of autowaves (Krinsky 1984).

Autowaves represent a particular class of nonlinear waves, which propagate in an active excitable media at the expense of the energy stored in the medium. The term 'autowaves' (Grekhova 1981) was coined by R. V. Khorhlov, as an abbreviation for 'autonomous waves', since such waves can propagate without a forcing function. Autowaves are manifestations of a strongly nonlinear active medium. They are self-sustained signals which induce a local release of stored energy in an active medium, and use it to trigger the same process in adjacent regions. Typical examples of autowaves include the waves of combustion, waves of phase transitions, concentration waves in chemical reactions (Zaikin & Zhabotinsky 1970; Pérez-Muñuzuri 1991), and many biological autowave processes (propagation of nerve impulses (Scott 1975), excitation waves in the cardiac muscle (Allesie *et al.* 1973), cultures of the slime

Phil. Trans. R. Soc. Lond. A (1995) **353**, 101–113
Printed in Great Britain

mould Dyctiostelium discoideum (Devreotes *et al.* 1983), epidemic waves in ecological communities (Anderson & May 1986), retinae (Bures *et al.* 1984), spreading waves in the cerebral cortex (Ermentrout & Cowan 1979), etc. These examples stress the importance of the autowave phenomena.

During the last few years, a lot of work has been done in the study of discretely coupled dynamical systems. For example, the coupling between a one-dimensional array of continuously stirred tank reactors has been used recently to prove the existence of travelling waves in such a medium (Laplante & Erneux 1992). Classical examples of discrete systems in nature include the nerves (Scott 1975), or linear arrays of cells connected among them by diffusion. An example in a two-dimensional medium is the propagation of electric pulses in the cardiac tissue (Allesie *et al.* 1973) (composed of cells connected by diffusion with the neighbouring cells). This propagation is responsible for the pumping of blood by the heart. Some anomalies can appear in their behaviour, such as the anchoring of a wave in an inhomogeneity of the medium (dead or damaged cell), or the formation of a discontinuous wave front when a region of the system (a group of cells) is re-excited almost immediately after the passage of a previous wave through that region (this phenomenon is called *vulnerability* (Spach *et al.* 1981; Starmer *et al.* 1992; Gómez-Gesteira *et al.* 1994)). In all of these cases the broken wave evolves into a spiral or vortex, which rotates in the heart imposing a higher frequency that eventually results in a disordered behaviour where the heart can no longer pump any blood, thereby leading to sudden death.

In recent years, it has become apparent that continuous models cannot account for all propagation phenomena occurring in nature. For example, biological experiments on nerve propagation show that a signal can fail to propagate under certain conditions, a situation that cannot occur if the medium is a homogeneous continuum. One of the most well-known examples is 'multiple sclerosis'. In this case, travelling wave propagation fails due to a lack of current needed to stimulate the excitable nerves. The study of wave propagation in systems of excitable cells is an important aspect of neurophysiology and cardiophysiology, see for example (Scott 1975). It is often the case that propagation failure (Keener 1987) leads to failure of these systems, and in the case of the cardiac action potential, this can be fatal (Cole *et al.* 1988).

In 1952 A. M. Turing suggested that, under certain conditions, chemicals can react and diffuse in such a way that it produces a steady state consisting of heterogeneous spatial patterns of chemical or morphogen concentrations. Turing structures have been suggested as a possible basis for morphogenesis in large-scale biological systems (Murray 1989). In the last few years, these structures have been shown experimentally to occur within starch-gels (Castets *et al.* 1990; Ouyang & Swinney 1991) which allow the separation of diffusion constants necessary for a Turing structure.

Hexagonal patterns constitute an important subject of research in the theory of Turing and convection structures (Ciliberto *et al.* 1988; De Kepper *et al.* 1994). However, perfect hexagonal patterns are rather difficult to observe in large systems. Typically, different line or point defects appear in the background of a hexagonal pattern. Among point defects, the so called 'penta-hepta' defects, or pair of cells with five and seven ridges, are the most typical. These defects, once having been created, are very stable (Ciliberto *et al.* 1990) and they separate multiple domains of hexagons having different orientations.

Arrays of nonlinear electronic circuits have been used to model reaction-diffusion systems and autowave propagation (Muñuzuri *et al.* 1993; Andronov *et al.* 1966; Feingold *et al.* 1988). Among them, Chua's circuit (Chua 1992; Madan 1993) has been

PHILOSOPHICAL TRANSACTIONS OF THE ROYAL SOCIETY A MATHEMATICAL, PHYSICAL & ENGINEERING SCIENCES

proven to be a very useful tool that can exhibit a very large variety of behaviours (see Muñuzuri *et al.* (1995) for a review).

Travelling, triggered or transition waves have been studied in one-dimensional arrays of electronic circuits. The results have been used to simulate the mechanism of propagation failure (Pérez-Muñuzuri *et al.* 1992), as well as for image processing applications (Pérez-Muñuzuri *et al.* 1993).

More complex patterns in a two-dimensional medium have been found and studied (Muñuzuri *et al.* 1993). Structures like spiral waves and targets exhibit a periodic behaviour in both space and time. Vortices are used to study the mechanism of their initiation (vulnerability) (Gómez-Gesteira *et al.* 1994).

Stable stationary patterns, such as Turing patterns (Pérez-Muñuzuri 1995), have also been found in two-dimensional arrays of discreetly coupled circuits. The interaction between these structures with an external forcing leads to a perfect organization of the pattern into a rhombic array, which is generic of any reaction-diffusion system undergoing a Turing bifurcation.

In this paper, we present a review of the structures and behaviours observed in arrays of Chua's circuits and some recently observed results and applications.

2. Model

The basic unit (cell) of our arrays is a Chua's circuit (Chua 1992; Madan 1993). The circuit contains three linear energy-storage elements (an inductor L, and two capacitors C_1 and C_2), a linear resistor with resistance $1/G$, and a nonlinear resistor, N_{R}, called Chua's diode. Each oscillator is coupled to its neighbours through linear resistors, thereby simulating a diffusion process.

The dynamics of the array of Chua's circuits can be modelled by a system of third-order autonomous nonlinear differential equations. In particular, we consider the dimensionless form of these equations (Muñuzuri *et al.* 1995),

$$\left.\begin{aligned}
\dot{x}_{i,j} &= \alpha(y_{i,j} - h(x_{i,j}) + D_{1x}(x_{i+1,j} + x_{i-1,j} - 2x_{i,j}) \\
&\quad + D_{1y}(x_{i,j+1} + x_{i,j-1} - 2x_{i,j}), \\
\dot{y}_{i,j} &= x_{i,j} - y_{i,j} + z_{i,j}) + D_{2x}(y_{i+1,j} + y_{i-1,j} - 2y_{i,j}) \\
&\quad + D_{2y}(y_{i,j+1} + y_{i,j-1} - 2y_{i,j}), \\
\dot{z}_{i,j} &= -\beta y_{i,j} - \gamma z_{i,j},
\end{aligned}\right\} \quad \begin{aligned} i &= 1, \ldots, N, \\ j &= 1, \ldots, M. \end{aligned} \tag{1}$$

The dimensionless equation of the three-segment piecewise- linear characteristic of the nonlinear resistor (Chua's diode) is given by $h(x) = a_0 + a_1 x + b_1|x - x_1| + b_2|x - x_2| + \epsilon$, where $a_1 = \frac{1}{2}(m_1 + m_2)$, $b_1 = \frac{1}{2}(m_0 - m_1)$, $b_2 = \frac{1}{2}(m_2 - m_0)$, $a_0 = b_1 x - b_2 x_2$ and ϵ accounts for the excitability of the system. We will choose $x_1 = -1$ and $x_2 = (m_0 - m_1)/(m_0 - m_2)$ so that the classical symmetrical situation (Chua 1992) is recovered when $m_2 = m_1$. In addition to (1), we impose zero-flux boundary conditions. A uniform time step of 0.001 was used throughout as the differential equations were integrated using an explicit Euler method.

The dimensionless parameters in (1) are related to the physical parameters by

$$D_{1x} = \frac{\alpha}{GR_{1x}}, \qquad D_{1y} = \frac{\alpha}{GR_{1y}}, \qquad D_{2x} = \frac{1}{GR_{2x}}, \qquad D_{2y} = \frac{1}{GR_{2y}},$$

$$G = \frac{1}{R}, \qquad \alpha = \frac{C_2}{C_1}, \qquad \beta = \frac{C_2}{LG^2}, \qquad \gamma = \frac{C_2 r_0}{LG},$$

$$m_0 = 1 + \frac{G_0}{G}, \qquad m_1 = 1 + \frac{G_1}{G}, \qquad m_2 = 1 + \frac{G_2}{G},$$

where r_0 is a small resistance introduced to account for the internal resistance of the physical inductor coil used in our experiments. G_0, G_1 and G_2 denote the slopes of the middle, left and right segments, respectively, of the nonlinear resistor N_{R}.

Note that two kinds of couplings are provided by two resistive grids made of resistors R_1 and R_2, respectively. They correspond to the two simplest methods to couple each Chua's circuit to its neighbours. We will henceforth refer to these two coupling methods as coupling across nodes N_1 and N_2, respectively. Usually, we choose $R_1 = R_{1x} = R_{1y}$ and $R_2 = R_{2x} = R_{2y}$ (for an isotropic two-dimensional medium). However, they are also allowed to vary in the case of an anisotropic medium, or in a one-dimensional medium ($R_{1y} = R_{2y} = \infty$).

3. Spiral waves in two-dimensional grids

A grid of 101×101 oscillators was used in our numerical calculations. The model parameters (C_1, C_2, r_0, L, G_1, G_2, G_0, G) were assigned the values (1 nF, 10 nF, $5\,\Omega^{-1}$, 0.04 H, $1.1 \times 10\,\Omega^{-1}$, $2.3 \times 10\,\Omega^{-1}$, $-0.5 \times 10\,\Omega^{-1}$, $0.9 \times 10\,\Omega^{-1}$) for both the excitable and the oscillating cases. The only difference between these two cases is the value of the offset, $\epsilon = 0$ and $\epsilon = 0.4$, respectively (Muñuzuri *et al.* 1993).

In an excitable or oscillating medium, waves propagate through it without disruption. Under certain circumstances this wave can be broken giving rise to a pair of free ends of the wave front that start propagating. This free end of the wave front sprouts in a direction perpendicular to the motion of the wave: it curls and evolves into a vortex.

To obtain a free end we have used the set of initial conditions described by Muñuzuri *et al.* (1993).

Figure 1 shows several snapshots depicting the dynamic process from the initial pattern to a fully developed spiral wave. Here, only the x variable is shown for the oscillating case. Figure 1*a* shows the initial conditions where all points inside the 'wedge-like' region correspond to the excited value in x (in this case $x = -2.9$, corresponding to the fast part in the limit cycle) and all other points correspond to an equilibrium value (slow part of the limit cycle). Observe that the tip of the wave front in figure 1*b* begins to increase its curvature. This process is seen to continue in figure 1*c*, *d*, where the number of turns of the spiral increases until it reaches the equilibrium. The configuration shown in figure 1*e* has reached a stationary state but continued rotating steadily for 1000 time units (TU) as shown in figure 1*f*.

A spiral wave is the stationary pattern with the highest frequency that a medium can spontaneously support. Once a spiral is created, all other structures such as target waves (i.e. a train of concentric circular waves, generally created by an inhomogeneity in the medium) will be swamped and eventually disappear. This is the mechanism in the cardiac muscle. Here, concentric waves are generated in the *atrial sinus* (located at the upper part of the heart) and propagate towards the opposite side as the muscle contracts periodically (pumping the blood). If one of the wave front breaks in the medium (by a vulnerability process, or other mechanisms) it will evolve into a pair of spiral waves with a frequency higher than the pumping frequency and will annihilate

PHILOSOPHICAL TRANSACTIONS OF THE ROYAL SOCIETY A MATHEMATICAL, PHYSICAL & ENGINEERING SCIENCES

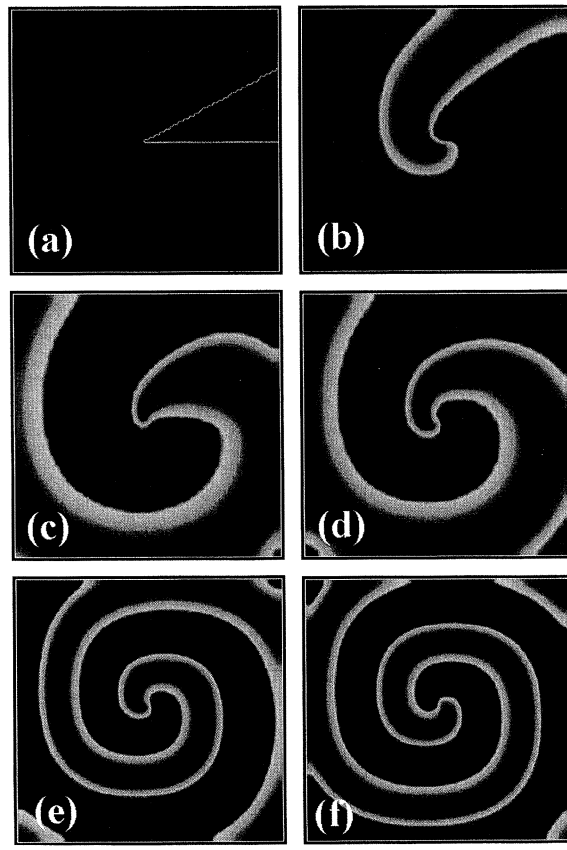

Figure 1. Time snapshots showing the birth of a fully developed spiral wave. Figures (a)–(f) correspond to 0, 10, 20, 50, 200 and 1000 time units (each time unit (TU) is equal to 0.105 ms in real physical time). For $t = 0$ the initial condition is shown. After $t = 1000$, the spiral structure remains while steadily rotating around the centre. In this case, the tip of the spiral follows a circular pattern (called the core) with a typical diameter of five circuits. Black colour in all figures corresponds to the minimum value of the x variable which, in this case, corresponds to the value of excitation. The grey colour corresponds to the maximum value of the x variable; namely, the resting state of the circuit.

any concentric waves created in the *atrial sinus* (this mechanism can, eventually, lead to the death of the organism if the vortex is not eliminated from the medium).

4. Turing structures

(*a*) *Conditions for Turing pattern formation*

Turing patterns are those stationary structures that appear spontaneously upon breaking the symmetry of the medium, and which resulted only from the coupling between the reaction and the diffusion processes (which contradicts the general idea that diffusion is a stabilizing process). In fact, these systems, in the absence of diffusion, tend to a linearly stable uniform steady state. Once Turing patterns arise, they remain stable until some external perturbation destroys them, but after that perturbation stops, Turing structures reappear and reorganize themselves.

Here, we use a two-dimensional array of Chua's circuits where each cell/unit is

PHILOSOPHICAL TRANSACTIONS OF THE ROYAL SOCIETY A MATHEMATICAL, PHYSICAL & ENGINEERING SCIENCES

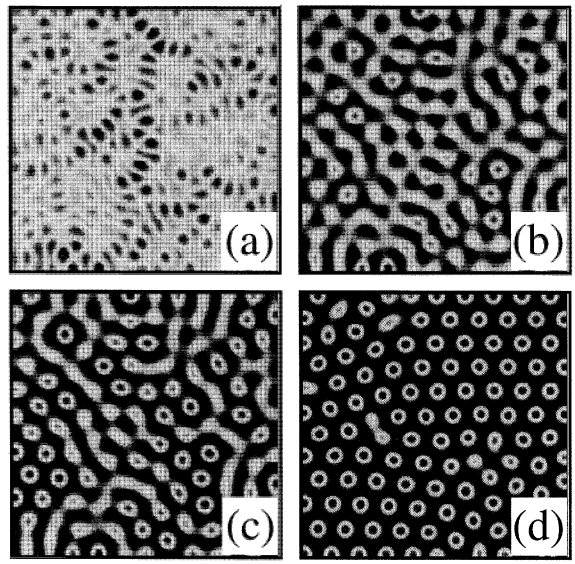

Figure 2. Temporal spontaneous formation of hexagonal arrays. Note the different orientations of the hexagon domains in (*d*) are separated by 'penta-hepta' defects. Size of the array: 100×100 and time of calculations: (*a*) 20 TU, (*b*) 70 TU, (*c*) 120 TU, (*d*) 2000 TU. ($D_1 = 1$ and $D_2 = 40$). In all figures, the centre of the blobs corresponds to the maximum value of the x variable in equation (1).

coupled to its four neighbours through resistors at its nodes N_1 and N_2 in equation (1). Experimental realization of these arrays will allow us to modify most of the parameters affecting Turing pattern formation, as well as to investigate long-range behaviours.

The set of fixed parameters satisfying Turing conditions which we used in this section is $\{\alpha, \beta, \gamma, m_0, m_1, m_2, \epsilon\} = \{-10, 10^{-3}, 10^{-3}, -1, 0.1, 0.1, 2\}$. A random initial condition was chosen for all variables in equation (1) so that $x_{i,j} \in [0.0, 4.5]$, $y_{i,j} \in [1.0, 1.3]$ and $z_{i,j}$ was kept constant and equal to $-\frac{9}{8}, \forall i, j = 1, \ldots, N$. D_{1y} and D_{2y} were set to zero and $D_{1x} = D_1$ and $D_{2x} = D_2$.

Figure 2*a–d* shows the temporal spontaneous formation of hexagonal lattices characterized by multiple domains, each of which contains a fairly uniform array with different orientations. Observe that different domains are separated by 'penta-hepta' defects. These defects, once having been created at the beginning of the simulation are very stable and remain motionless (figure 2*d*).

(*b*) *Sidewall forcing of hexagonal Turing patterns*

The effect of imposed spatial or temporal modulations on pattern-forming systems has been analysed recently in various experimental and theoretical situations (Coullet & Walgraef 1989; Cross & Hohenberg 1993).

On the other hand, although the effect of global spatial or temporal modulation have been widely studied, little has been done on the effect of local forcing on Turing structures. Periodic sidewall forcing on Turing patterns mimics the behaviour of the boundary between two domains; one, where periodic wave trains propagate through the medium and the other, where Turing structures are developing.

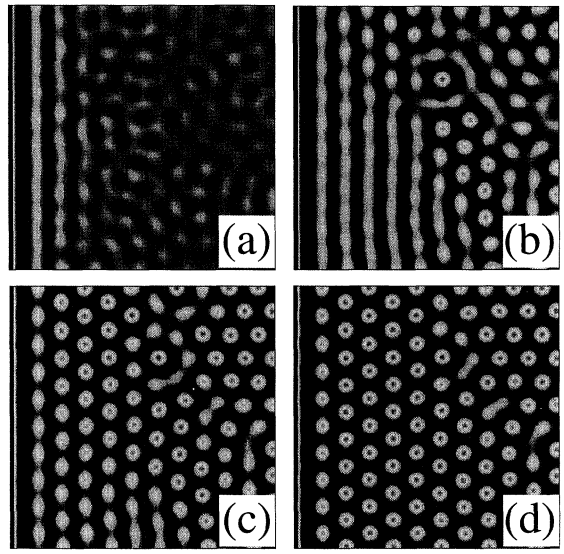

Figure 3. Temporal evolution of a coexisting state of rhombi and hexagons. Those columns of blobs at the left of the figure are periodically stretched and expanded giving rise during the first few iterations to (*a*) rolls oriented along the left boundary and blobs that begin to develop far from it. These patterns will eventually evolve into rhombi (first five columns of blobs at the left of the figure), (*b*) and hexagons (last five columns), (*c*) separated from the rest by 'penta-hepta' defects. The parameters are: $A_p = 2$, $\omega = 0$, $D_1 = 1$, $D_2 = 39$). Iteration times: (*a*) 50 TU, (*b*) 300 TU, (*c*) 600 TU, (*d*) 2000 TU.

The periodic sidewall forcing to the system was modelled by adding the term

$$A_p \cos(\omega t)\delta(i-1) \tag{2}$$

to equation (1) for the x variable, where A_p and ω are the amplitude and frequency of forcing, respectively, and $\delta(\cdot)$ is the Dirac's delta which is equal to one when $i = 1$ for any $j \in [1, n]$, and zero otherwise.

We have observed that when a periodic sidewall forcing is applied with the same initial state which leads to figure 2, perfect organization into a rhombic array is obtained. This state is characterized by wave vectors $\boldsymbol{k}_1$, $\boldsymbol{k}_2$ and $\boldsymbol{k}_3$ satisfying the resonant condition that $\boldsymbol{k}_1$ is perpendicular to the direction of forcing and $|\boldsymbol{k}_2| = |\boldsymbol{k}_3| \neq |\boldsymbol{k}_1|$. Besides, it was found that perfect organization of rhombi occurs only for specific values of D_1 and D_2 and some forcing frequency ω. Hence, we will assume from now on that locking between the forcing frequency and D_2 (characterized by some spatial frequency) occurs at some specific values of ω and D_2. This *resonance effect* is manifested by a perfect organization of rhombi obeying the Farey sequence (Pérez-Muñuzuri *et al.* 1995).

The evolution process leading to a coexisting state of rhombi and hexagons is shown in figure 3 at four different times. Observe that the first columns of blobs at the left of the figures are periodically expanded and contracted due to the forcing. From the first iterations, vertical stripes developed close to the left boundary while disordered blobs appear far from it. When the pattern becomes stationary in time, the stripes have developed into rhombi (they are detected by extracting this part of the image and obtaining its Fourier transform) and hexagons (far from the left boundary), separated by 'penta-hepta' defects.

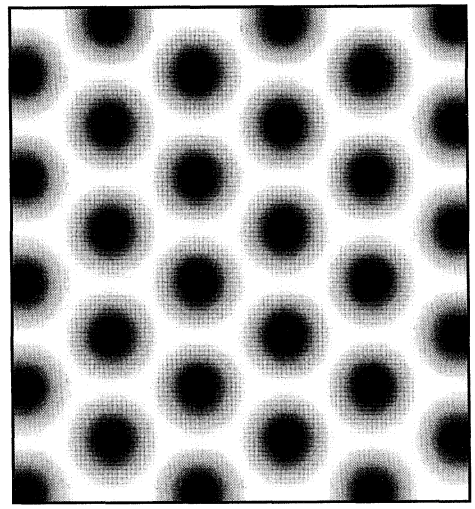

Figure 4. The rhombi stable pattern remains unchanged even after switching off the periodic sidewall forcing. This pattern remained stable (no defects appeared) throughout the calculation time period (50 000 TU). The parameters are: $A_p = 0$, $\omega = 0$, $D_1 = 1$ and $D_2 = 40$.

Any stable pattern obtained by sidewall forcing remains stable upon switching off the forcing ($A_p = 0$), as well as to slight perturbations on the forcing parameters, ω and A_p. For example, if after obtaining a perfectly organized rhombi (above 10 000 TU), the forcing was suppressed ($A_p = 0$ in equation (2)), we would find the perfectly organized rhombi (figure 4) remained unchanged. The new pattern, without forcing, remains stable over the remaining time duration (50 000 TU) of our computer simulation. This result suggests the possibility of controlling spatial defects via temporary sidewall forcings.

Rhombic arrays have been observed experimentally (Ouyang *et al.* 1993) and numerically (Dufiet & Boissonade 1992) in reaction-diffusion systems under spontaneous conditions for values of control parameters chosen close to those for hexagonal pattern formation (usually found with 'penta-hepta' defects).

(*c*) *Competition between Turing and Hopf modes*

In view of the discrete nature of our system, it is quite reasonable to study the interaction between different modes as well as to simulate inhomogeneities into the system. Here we present the simulations of two layers of Chua's circuits connected with resistive connections between them at both nodes. Equivalent experimental setups that are now currently used consist of a thin reacting layer, where the concentrations of the control species are fixed at the boundaries (Noszticzius *et al.* 1987; Castets *et al.* 1990). In this case, transverse concentration gradients are induced in the active medium, and may lead to the unfolding of the bifurcations and to the spatial coexistence of spatio-temporal patterns of different symmetries where these gradients can be considered as external forcing terms (Kramer *et al.* 1994).

In our simulations, each cell/unit is connected to its four nearest neighbours through nodes N_1 and N_2 in the same layer and to one neighbour in the opposite layer. The coupling between layers (D_1^v and D_2^v) induces in the system a characteristic length which accounts for the 'distance' between layers. Thus, for example, by increasing the coupling resistance between layers, the 'distance' between them increases and the interaction between the structures arising in both layers diminishes.

PHILOSOPHICAL TRANSACTIONS OF THE ROYAL SOCIETY A MATHEMATICAL, PHYSICAL & ENGINEERING SCIENCES

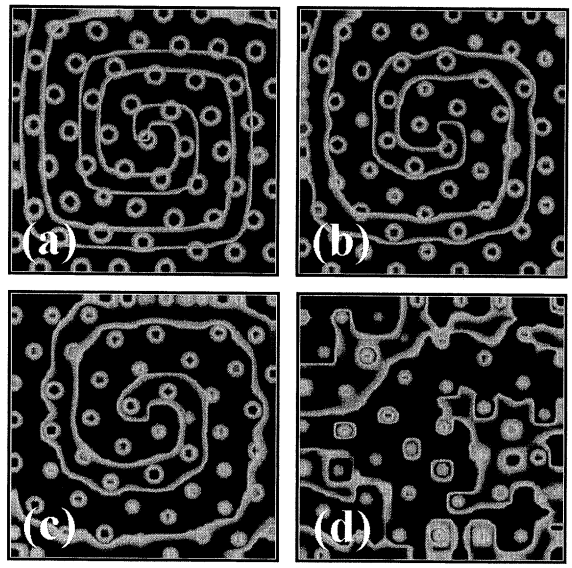

Figure 5. Interaction between Turing patterns and spiral waves. All images show the superposition of the two layers corresponding to the Turing and the Hopf modes, respectively. As the diffusion between layers is increased, from (*a*) to (*d*) (i.e. the distance between them is decreased), the period of the spiral wave increases and the size of the blobs decreases. Note that the core of the spiral always coincides with a blob in the Turing layer. Parameters and grey scale for the Turing patterns are as in figure 2, and for the spiral waves as in figure 1. The diffusion coefficients between layers ($D_2^v = 0.0$) are: (*a*) $D_1^v = 0.02$, (*b*) $D_1^v = 0.10$, (*c*) $D_1^v = 0.15$, (*d*) $D_1^v = 0.25$.

In this case, we study the interaction between Turing structures (Turing mode) and vortices (Hopf mode). Parameters and initial conditions for spiral waves and Turing patterns were chosen from those described above. Since the Turing pattern develops faster than a spiral wave, we choose a fully developed vortex as initial condition for the Hopf layer in order to study the interaction between the two modes.

Figure 5 shows the superposition of the patterns developing in the two layers (hexagons and spiral waves) after 1000 TU when the diffusion between layers, D_1^v, is increased for a constant value of $D_2^v = 0$. For small coupling coefficients the dynamics of both layers is not affected, see for example figure 5*a* for $D_1^v = 0.02$. As we increase the diffusion coefficient D_1^v, the period of the spiral waves increases while the size of the blobs in the Turing layer decreases, as shown in figure 5*b*, *c* (note that the wave length remains constant). Besides, the shape of the spiral waves becomes more unstable, and the number of defects in the Turing layer increases. Finally, for $D_1^v > 0.20$ (figure 5*d*), the spiral breaks down. Above this value, Turing and Hopf modes are mixed and they propagate in both layers. By increasing the diffusion between layers, the Hopf mode (waves) dominates the entire system. In all cases, it was observed that the tip of the spiral wave remained always anchored to a blob of the hexagonal pattern.

5. Coexistence of low- and high-dimensional spatio-temporal chaos

A one-dimensional array of Chua's circuit was used to investigate the appearance of spatio-temporal chaos (Zheleznyak & Chua 1994). The set of fixed parameters we

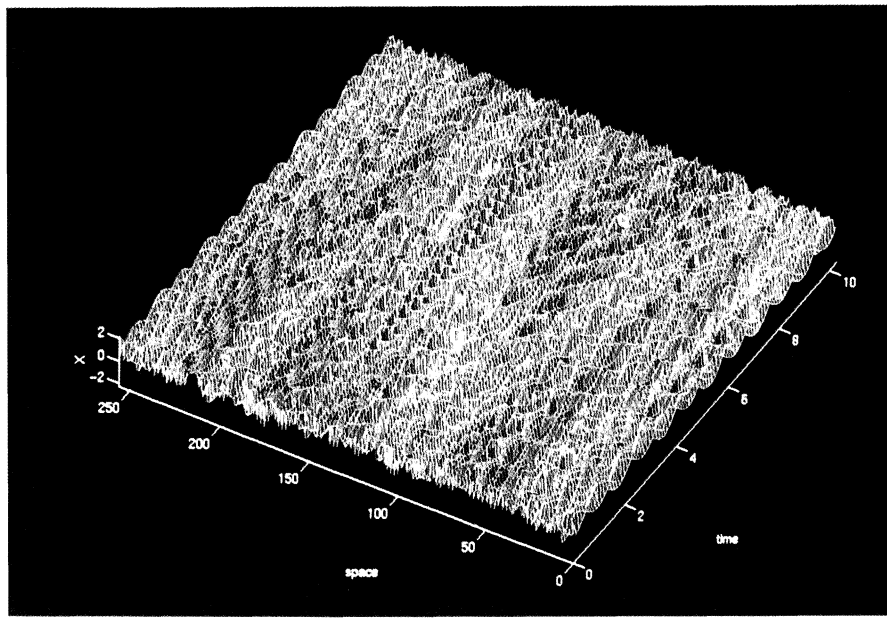

Figure 6. Chaotic spatio-temporal pattern of the variable x for initial conditions (3) and diffusion coefficient $D_{1x} = 0.4$.

used in this section is $\{\alpha, \beta, \gamma, m_0, m_1, m_2, \epsilon\} = \{9, 19, 0, -\frac{8}{7}, -\frac{5}{7}, -\frac{5}{7}, 0\}$. To obtain a one-dimensional medium D_{1y}, D_{2x} and D_{2y} were set to zero in equation (1) and D_{1x} was used as the bifurcation parameter. Periodic boundary conditions were used through all the calculations: $x_1 = x_{N+1}$, $y_1 = y_{N+1}$, $z_1 = z_{N+1}$, with $N \gg 1$.

The parameters for an uncoupled Chua's circuit were chosen so that it has two stable limit cycles, symmetrical with respect to the origin. Despite the simple local dynamics of the basic cell, the global behaviour of the system can be very complicated. The dynamics were studied for two types of initial conditions. In the first type,

$$x_i(0) = 1 + 0.1 \sin(2\pi(i-1)/N), \quad y_i(0) = z_i(0) = 0.1, \tag{3}$$

the trajectories of all cells are attracted to the same limit cycle. In the second type:

$$x_i(0) = \sin(2\pi(i-1)/N), \quad y_i(0) = z_i(0) = 0.1, \tag{4}$$

the trajectories of all cells belong to the basins of attractions of two different limit cycles. The computations showed that for both types of initial conditions, the dynamics of the system have much in common. For weak coupling, the spatio-temporal patterns in both cases are simple: weakly inhomogeneous in space and periodic in time. When the diffusion coefficient D_{1x} exceeds some critical value D_{cr}, a pattern occurs – so-called π-spatial oscillation – where almost all adjacent cells are 180° out of phase. Increasing the diffusion coefficient D_{1x} further gives rise to envelope waves against a background of π-oscillations and finally, when $D_{1x} \geqslant 0.33$, chaotic spatio-temporal patterns appear. We can see that these patterns no longer exhibit any regular structures in space and are chaotic (with broadband power spectrum) in time. Chaotic spatio-temporal patterns were further studied (Zheleznyak & Chua 1994) based on a new approach for describing the properties of patterns through

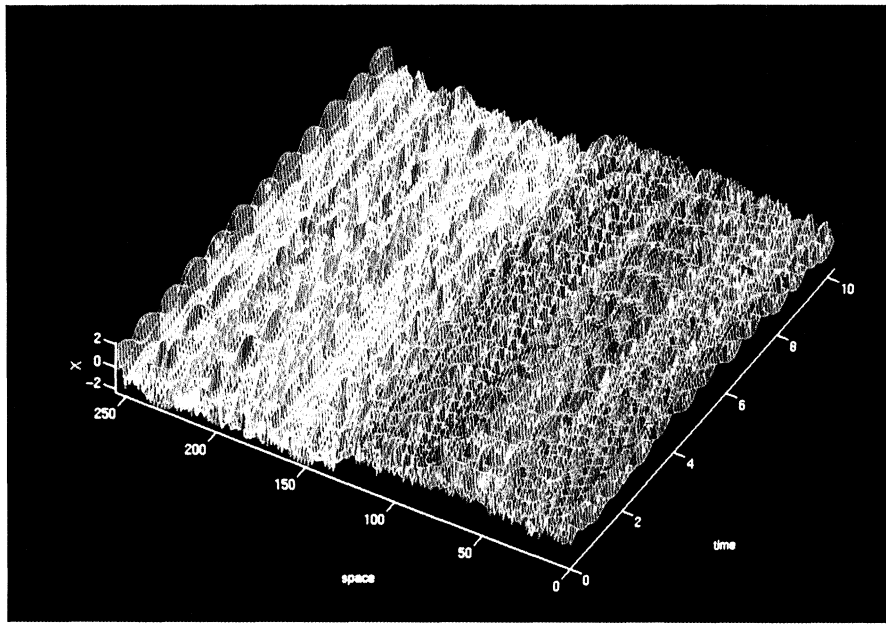

Figure 7. Result corresponding to figure 6 for initial condition (4).

the characteristics of associated attractors of a multidimensional dynamical system with a *matrix* phase space. Using this approach it has been found that the attractors corresponding to the chaotic patterns for initial conditions (3) (figure 6) have large correlation dimension (> 10), whereas for initial conditions (4) (figure 7) the correlation dimension is low (< 5). Thus it is shown that in the matrix phase space of CNNs, different high- and low-dimensional attractors coexist, corresponding to different initial conditions.

6. Conclusions

Throughout this paper we have demonstrated how an array of Chua's circuits provides a very useful tool for studying spatio-temporal patterns. A medium composed of diffusively coupled Chua's circuits results in a discrete system that mimics the behaviour observed in many natural systems; e.g. cardiac muscle, nerve fibres, Belousov–Zhabotinsky reaction, etc. This electronic system (CNN) can be built and controlled, because the parameters can be adjusted and measured with precision (and hence, its results are easily reproducible).

The CNN architecture has been shown to be able to support a great variety of solutions, as well as all known spatio-temporal structures observed from other (discrete or continuous) systems; spatio-temporal chaotic regimes, spiral waves, Turing patterns, interaction between Turing and Hopf modes.

Numerical calculations have been performed on the Vectorial Super Computer Fujitsu VP2400 at Centro de Supercomputación de Galicia, CESGA (Galicia, Spain). This work was supported in part by the Xunta de Galicia (Spain) under consecutive projects number XUGA20610B92 and XUGA20611B93, and by the USA Joint Services Electronics Program under contract no. F49620-93-C-0014.

References

Allesie, M. A., Bonke, F. I. M. & Scopman, T. Y. G. 1973 Circus movement in rabbit atrial muscle as a mechanism in tachycardia. *Circulation Res.* **33**, 54–62.

Anderson, R. M. & May, R. M. 1986 The invasion, persistence and spread of infectious diseases within animal and plant communities. *Phil. Trans. R. Soc. Lond.* B **314**, 533–570.

Andronov, A. A., Vitt, E. A. & Chaikin, S. E. 1966 *Theory of oscillators.* Oxford: Pergamon.

Bures, J., Koroleva, V. I. & Gorelova, N. A. 1984 Leao's spreading depression, an example of diffusion-mediated propagation of excitation in the central nervous system. In *Autowaves and structures far from equilibrium* (ed. V. I. Krinsky), pp. 180–183. Springer.

Castets, V., Dulos, E., Boissonade, J. & De Kepper, P. 1990 Experimental evidence of a sustained Turing-type nonequilibrium chemical pattern. *Phys. Rev. Lett.* **64**, 2953– 2956.

Chua, L. O. 1992 The genesis of Chua's circuits. *Int. J. Electron. Commun.* **46**, 250–257.

Ciliberto, S., Pampaloni, E. & Pérez–García, C. 1988 Competition between different symmetries in convective patterns. *Phys. Rev. Lett.* **61**, 1198–1201.

Ciliberto, S., Coullet, P., Lega, J., Pampaloni, E. & Pérez-García, C. 1990 Defects in roll-hexagon competition. *Phys. Rev. Lett.* **65**, 2370–2373.

Cole, W. C., Picolne, J. B. & Sperelakis, N. 1988 Gap junction uncoupling and discontinuous propagation in the heart. *Biophys. J.* **53**, 809–818.

Coullet, P. & Walgraef, D. 1989 Spatial forcing of 2D wave patterns. *Europhys. Lett.* **10**, 525–531.

Cross, M. C. & Hohenberg, P. C. 1993 Pattern formation outside of equilibrium. *Rev. mod. Phys.* **65**, 851–1112.

De Kepper, P., Perraud, J. J., Rudovics, B. & Dulos, E. 1994 Experimental study of stationary Turing patterns and their interaction with traveling waves in a chemical system. *Int. J. Bifurc. Chaos* **4**, 1215–1231.

Devreotes, P. N., Potel, M. J. & MacKay, S. A. 1983 Quantitative analysis of cyclic amp waves mediating aggregation in Dyctiostelium discoideum. *Devel. Biol.* **96**, 405–415.

Dufiet, V. & Boissonade, J. 1992 Numerical studies of Turing patterns selection in a two-dimensional system. *Physica* **188A**, 158–171.

Ermentrout, G. B. & Cowan, J. 1979 A mathematical theory of visual hallucination patterns. *Biol. Cybern.* **34**, 137–150.

Feingold, M., González, D. L., Piro, O. & Viturro, H. 1988 Phase locking, period doubling and chaotic phenomena in externally driven excitable systems. *Phys. Rev.* A **37**, 4060– 4063.

Glass, L. & Mackey, M. C. 1988 *From clocks to chaos: the rhythms of life.* Princeton University Press.

Gómez-Gesteira, M., Fernández-García, G., Muñuzuri, A. P., Pérez-Muñuzuri, V., Krinsky, V. I., Starmer, C. F. & Pérez-Villar, V. 1994 Vulnerability in excitable Belousov–Zhabotinsky medium: from 1D to 2D. *Physica* **76D**, 359–368.

Grekhova, M. T. 1981 Autowave processes in systems with diffusion. *Gorki Acad. Sci. USSR.*

Haken, H. 1983 *Advanced synergetics.* Springer.

Keener, J. P. 1987 Propagation and its failure in coupled systems of discrete excitable cells. *SIAM J. Appl. Math.* **47**, 556–572.

Kramer, L., Hynne, F., Sorenson, P. G. & Walgraef, D. 1994 The Ginzburg–Landau approach to oscillatory media. *Chaos* **4**, 443–452.

Krinsky, V. I. 1984 Autowaves: results, problems, outlooks. In *Self-organization: autowaves and structures far from equilibrium* (ed. V. I. Krinsky), pp. 9–19. New York: Springer.

Laplante, J. P. & Erneux, T. 1992 Propagation failure in arrays of coupled bistable chemical reactors. *J. Phys. Chem.* **96**, 4931–4934.

Madan, R. N. (ed.) 1993 *Chua's circuit: a paradigm for chaos.* World Scientific Series on Nonlinear Science, series B, vol. 1. Singapore: World Scientific.

Muñuzuri, A. P., Pérez-Muñuzuri, V., Pérez-Villar, V. & Chua, L. O. 1993 Spiral waves on a 2-D array of nonlinear circuits. *IEEE Trans. Circuits Systems* **40**, 872–877.

PHILOSOPHICAL TRANSACTIONS OF THE ROYAL SOCIETY A MATHEMATICAL, PHYSICAL & ENGINEERING SCIENCES

Muñuzuri, A. P., Pérez-Muñuzuri, V., Gómez-Gesteira, M., Chua, L. O. & Pérez-Villar, V. 1995 Spatio-temporal structures in discretely-coupled arrays of nonlinear circuits: a review. *Int. J. Bifurc. Chaos* **5**, 17–50.

Murray, J. D. 1989 *Mathematical biology.* New York: Springer.

Noszticzius, Z., Horsthemke, W., McCormick, W. D., Swinney, H. L. & Tam, W. Y. 1987 Sustained chemical waves in an annular gel reactor: a chemical pinwheel. *Nature, Lond.* **329**, 619–621.

Ouyang, Q. & Swinney, H. L. 1991 Transitions from a uniform state of hexagonal and striped Turing patterns. *Nature, Lond.* **352**, 610–612.

Ouyang, Q., Gunaratne, G. H. & Swinney, H. L. 1993 Rhombic patterns: broken hexagonal symmetry. *Chaos* **3**, 707–711.

Perez-Muñuzuri, V., Aliev, R., Vasiev, V., Pérez-Villar, V. & Krinsky, V. I. 1991 Super-spiral structures in an excitable medium. *Nature, Lond.* **353**, 740–742.

Pérez-Muñuzuri, V., Pérez-Villar, V. & Chua, L. O. 1992 Propagation failure in linear arrays of Chua's circuits. *Int. J. Bifurc. Chaos* **2**, 403–406.

Pérez-Muñuzuri, V., Pérez-Villar, V. & Chua, L. O. 1993 Autowaves for image processing on a two-dimensional CNN array of excitable nonlinear circuits: flat and wrinkled labyrinths. *IEEE Trans. Circuits Systems* **40**, 174–181.

Pérez-Muñuzuri, V., Gómez-Gesteira M., Muñuzuri, A. P., Chua, L. O. & Pérez-Villar, V. 1995 Sidewall forcing of hexagonal Turing patterns: rhombic patterns. *Physica* **82D**, 195–204.

Scott, A. C. 1975 The electrophysics of a nerve fiber. *Rev. mod. Phys.* **47**, 487–533.

Spach, M. S., Miller, W. T., Geselowitz, D. B., Borr, R. C., Kootsey, J. M. & Johnson, E. A. 1981 The discontinuous nature of propagation in normal canine cardiac muscle. Evidence for recurrent discontinuities of intracellular resistence that affect the membrane currents. *Circ. Res.* **48**, 39–54.

Starmer, C. F., Biktashev, V. N., Romaksho, D. N., Stepanov, M. N., Makarova, O. N. & Krinsky, V. I. 1992 Vulnerability in excitable medium: analytical and numerical studies of initiating unidirectional propagation. *Biophys. J.* **65**, 1775–1787.

Turing, A. M. 1952 The chemical basis of morphogenesis. *Phil. Trans. R. Soc. Lond.* B **327**, 37–72.

Winfree, A. T. 1987 *When time breaks down.* Princeton University Press.

Zaikin, A. N. & Zhabotinskii, A. M. 1970 Concentration wave propagation in two-dimensional liquid phase self-organizing system. *Nature, Lond.* **225**, 535–537.

Zheleznyak, A. L. & Chua, L. O. 1994 Coexistence of low- and high-dimensional spatio-temporal chaos in a chain of dissipatively coupled Chua's circuit. *Int. J. Bifurc. Chaos* **4**, 639–674.

Zykov, V. S. 1987 *Simulation of wave processes in excitable media.* Manchester University Press.

PHILOSOPHICAL TRANSACTIONS OF THE ROYAL SOCIETY A MATHEMATICAL, PHYSICAL & ENGINEERING SCIENCES

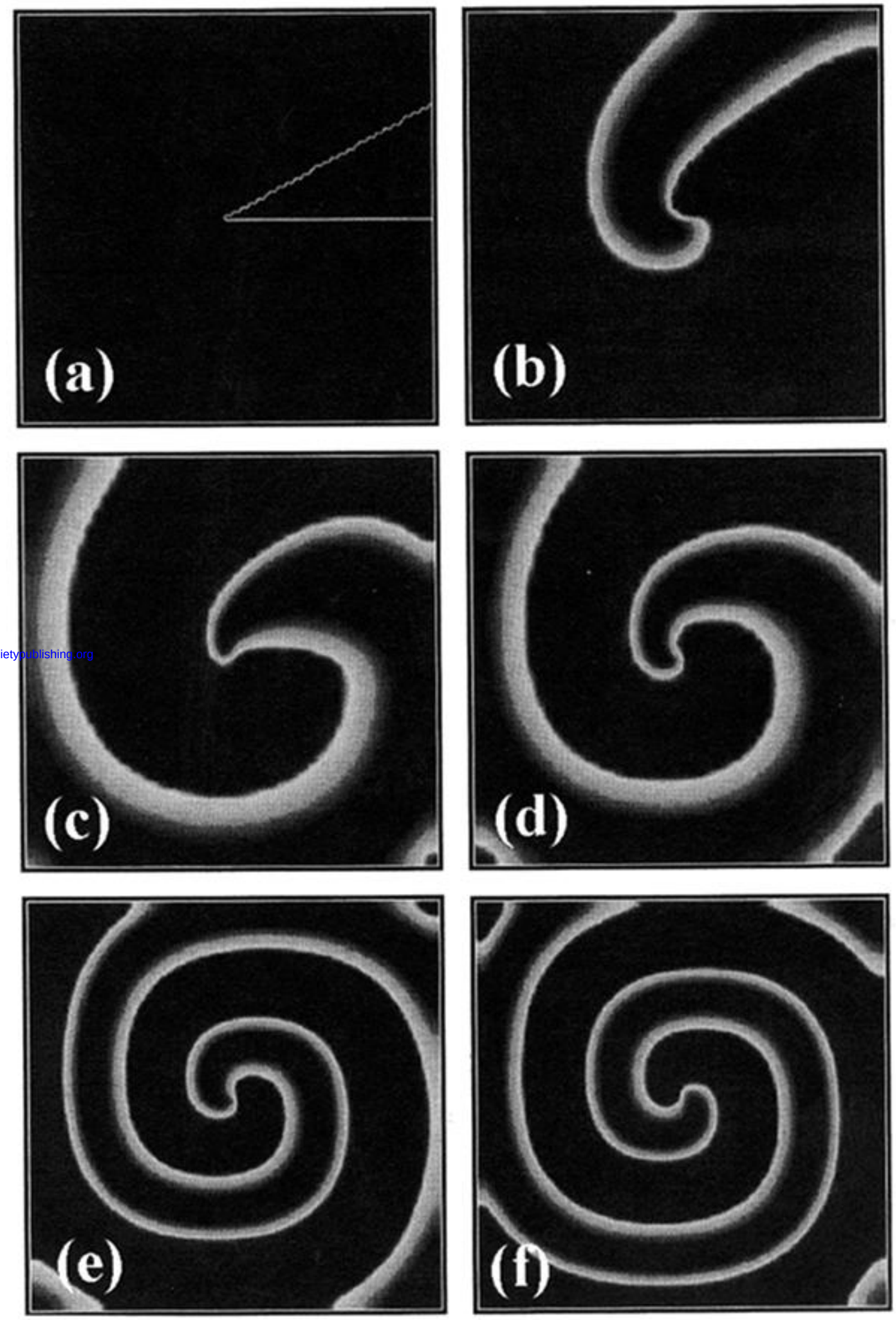

Figure 1. Time snapshots showing the birth of a fully developed spiral wave. Figures (*a*)–(*f*) correspond to 0, 10, 20, 50, 200 and 1000 time units (each time unit (TU) is equal to 0.105 ms in real physical time). For $t = 0$ the initial condition is shown. After $t = 1000$, the spiral structure remains while steadily rotating around the centre. In this case, the tip of the spiral follows a circular pattern (called the core) with a typical diameter of five circuits. Black colour in all figures corresponds to the minimum value of the x variable which, in this case, corresponds to the value of excitation. The grey colour corresponds to the maximum value of the x variable; namely, the resting state of the circuit.

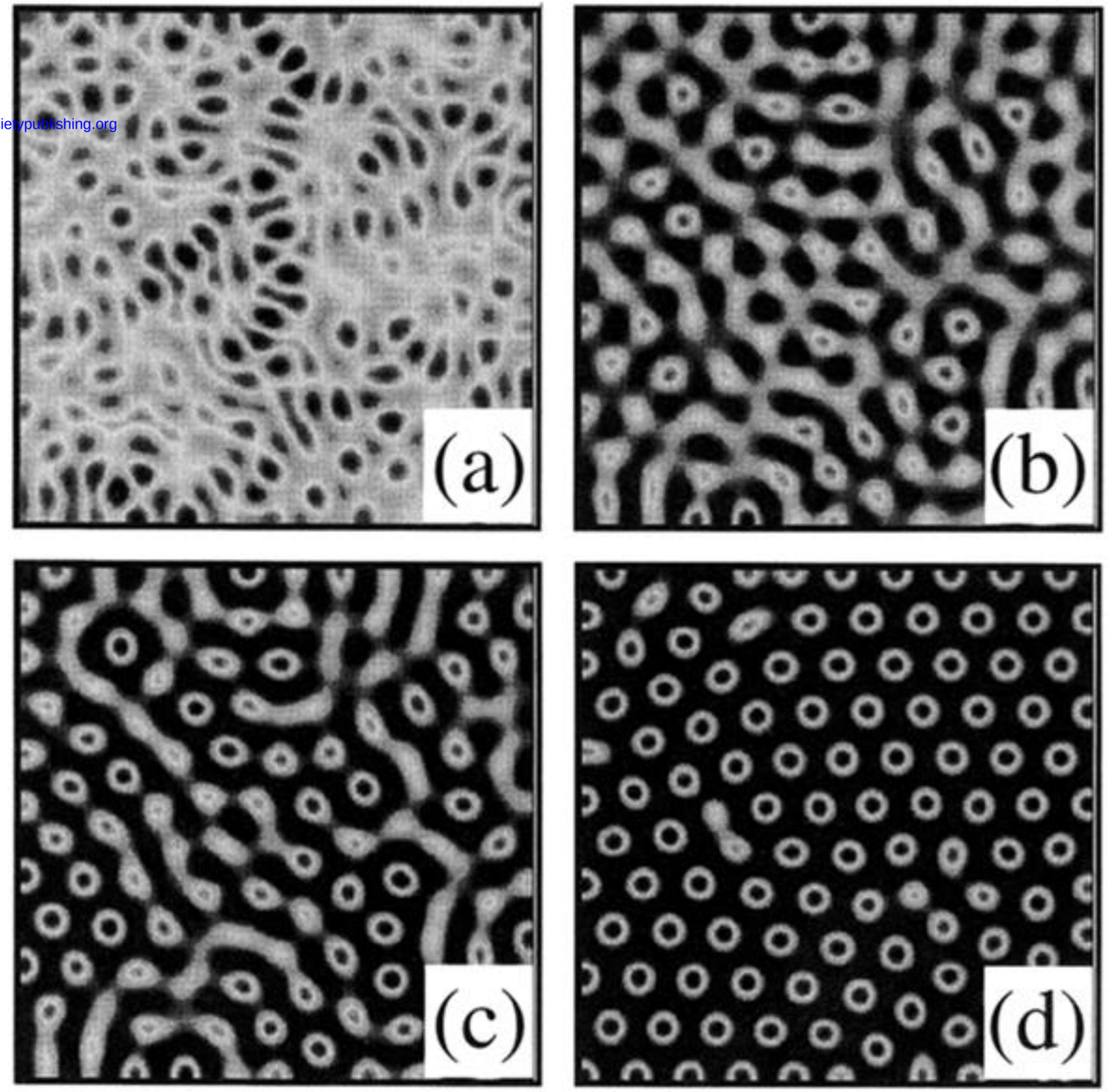

igure 2. Temporal spontaneous formation of hexagonal arrays. Note the different orientations
the hexagon domains in (*d*) are separated by 'penta-hepta' defects. Size of the array: 100×100
id time of calculations: (*a*) 20 TU, (*b*) 70 TU, (*c*) 120 TU, (*d*) 2000 TU. ($D_1 = 1$ and $D_2 = 40$).
all figures, the centre of the blobs corresponds to the maximum value of the x variable in
quation (1).

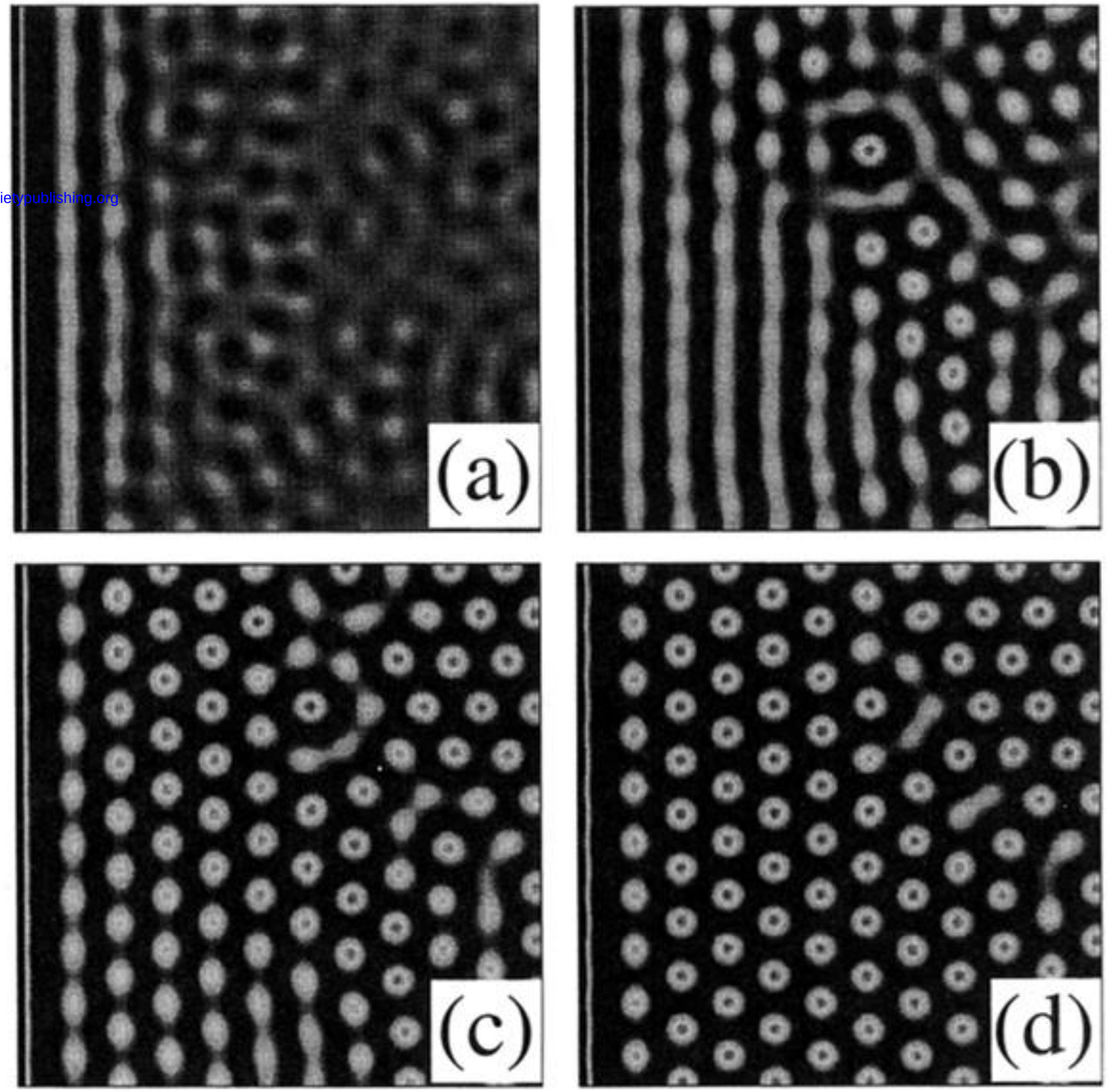

igure 3. Temporal evolution of a coexisting state of rhombi and hexagons. Those columns of obs at the left of the figure are periodically stretched and expanded giving rise during the first w iterations to (*a*) rolls oriented along the left boundary and blobs that begin to develop far om it. These patterns will eventually evolve into rhombi (first five columns of blobs at the left the figure), (*b*) and hexagons (last five columns), (*c*) separated from the rest by 'penta-hepta' efects. The parameters are: $A_p = 2$, $\omega = 0$, $D_1 = 1$, $D_2 = 39$). Iteration times: (*a*) 50 TU, (*b*) 00 TU, (*c*) 600 TU, (*d*) 2000 TU.

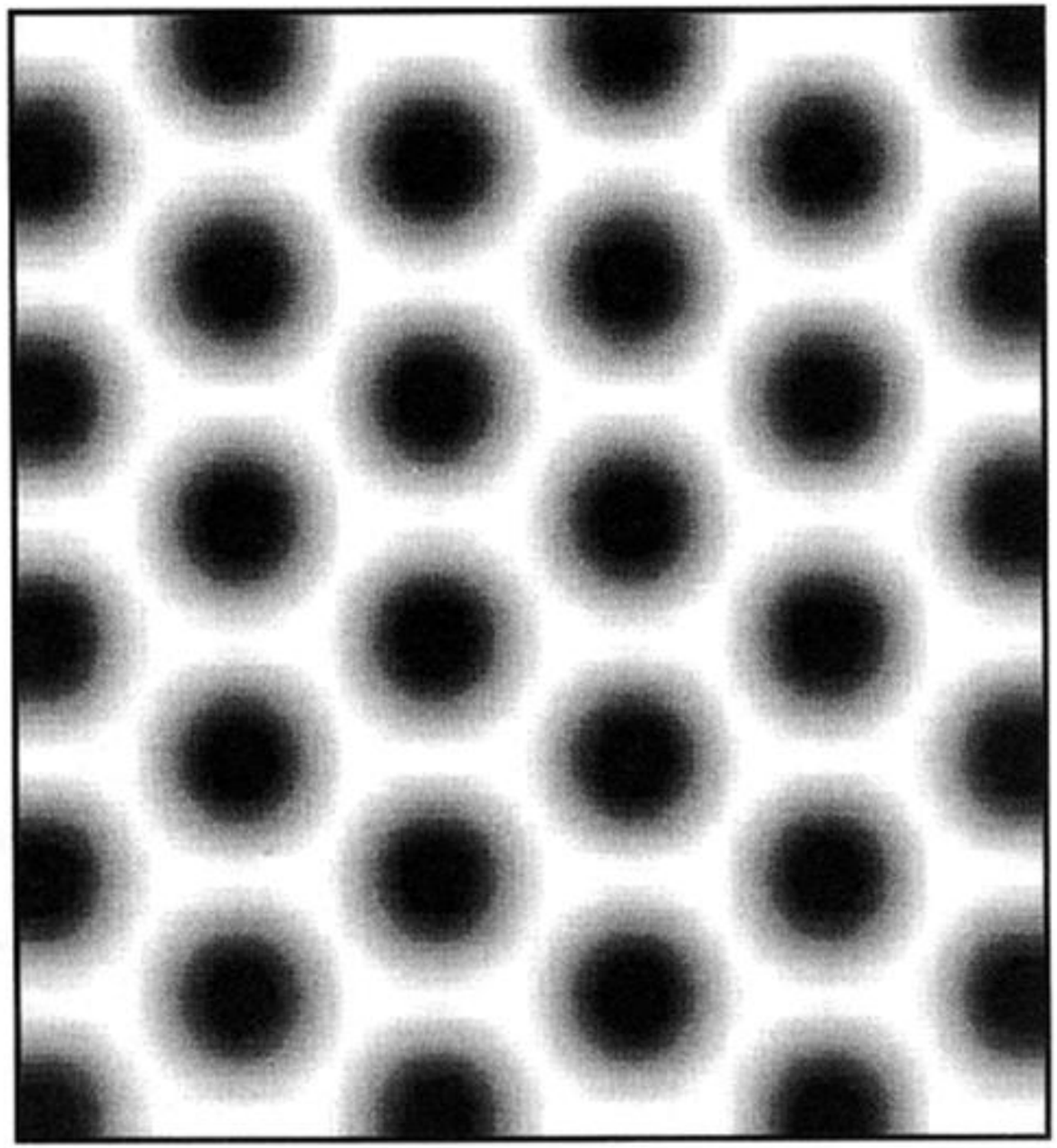

igure 4. The rhombi stable pattern remains unchanged even after switching off the periodic dewall forcing. This pattern remained stable (no defects appeared) throughout the calculation me period (50 000 TU). The parameters are: $A_p = 0$, $\omega = 0$, $D_1 = 1$ and $D_2 = 40$.

PHILOSOPHICAL TRANSACTIONS OF THE ROYAL SOCIETY A MATHEMATICAL, PHYSICAL & ENGINEERING SCIENCES

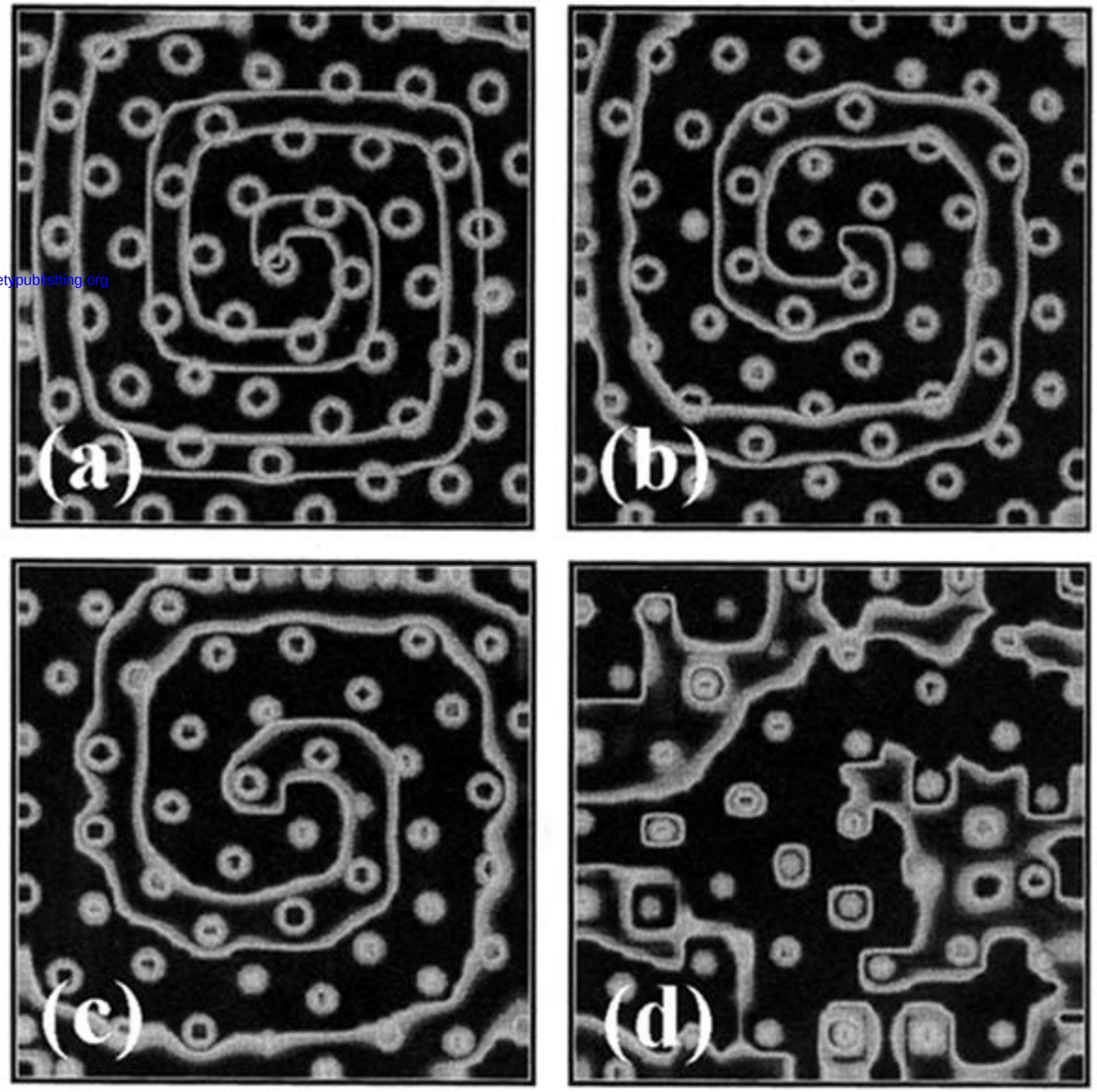

gure 5. Interaction between Turing patterns and spiral waves. All images show the super-osition of the two layers corresponding to the Turing and the Hopf modes, respectively. As e diffusion between layers is increased, from (a) to (d) (i.e. the distance between them is de-eased), the period of the spiral wave increases and the size of the blobs decreases. Note that e core of the spiral always coincides with a blob in the Turing layer. Parameters and grey scale r the Turing patterns are as in figure 2, and for the spiral waves as in figure 1. The diffusion efficients between layers ($D_2^v = 0.0$) are: (a) $D_1^v = 0.02$, (b) $D_1^v = 0.10$, (c) $D_1^v = 0.15$, (d) $_1^v = 0.25$.

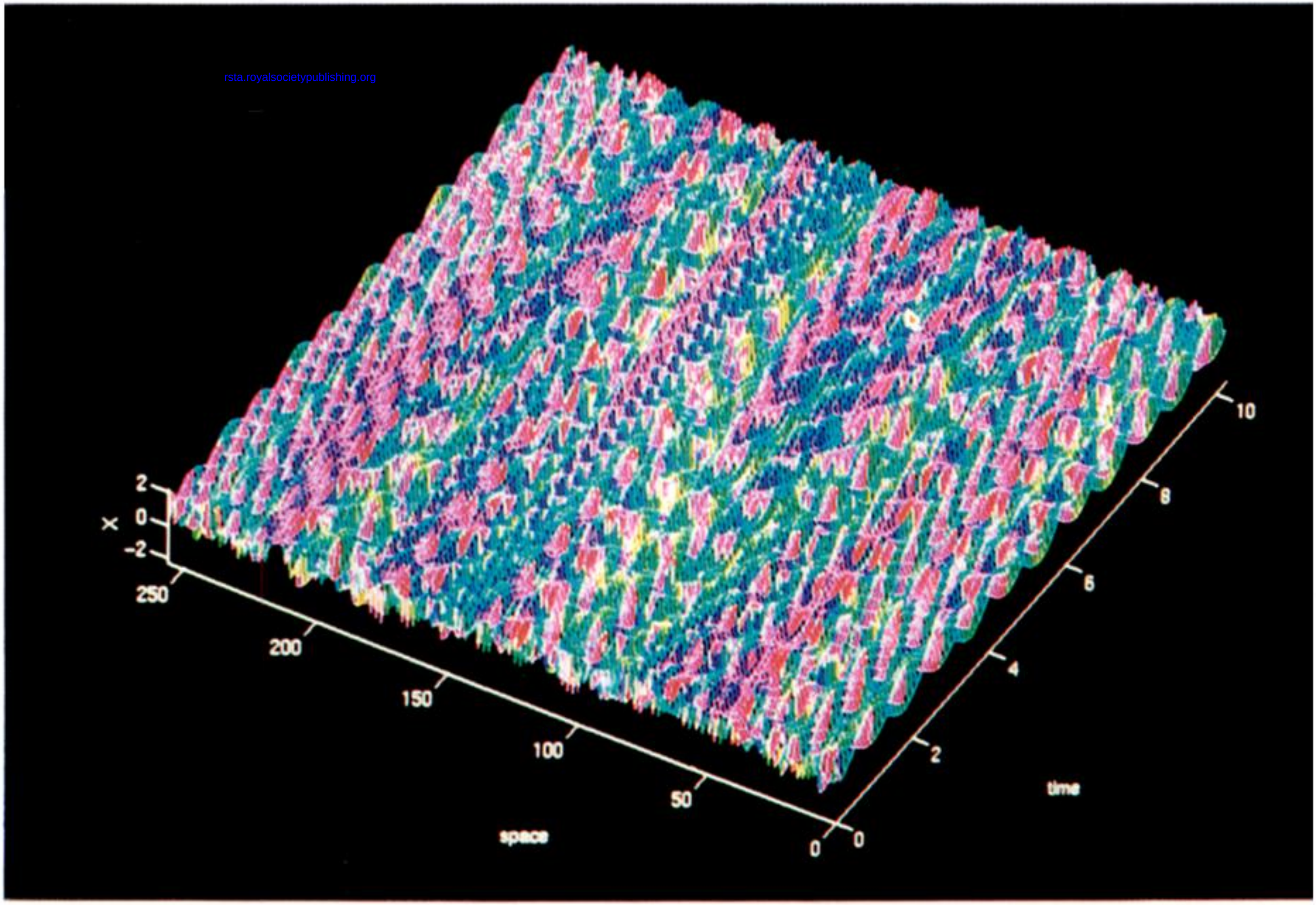

gure 6. Chaotic spatio-temporal pattern of the variable x for initial conditions (3) and diffusion coefficient $D_{1x} = 0.4$.

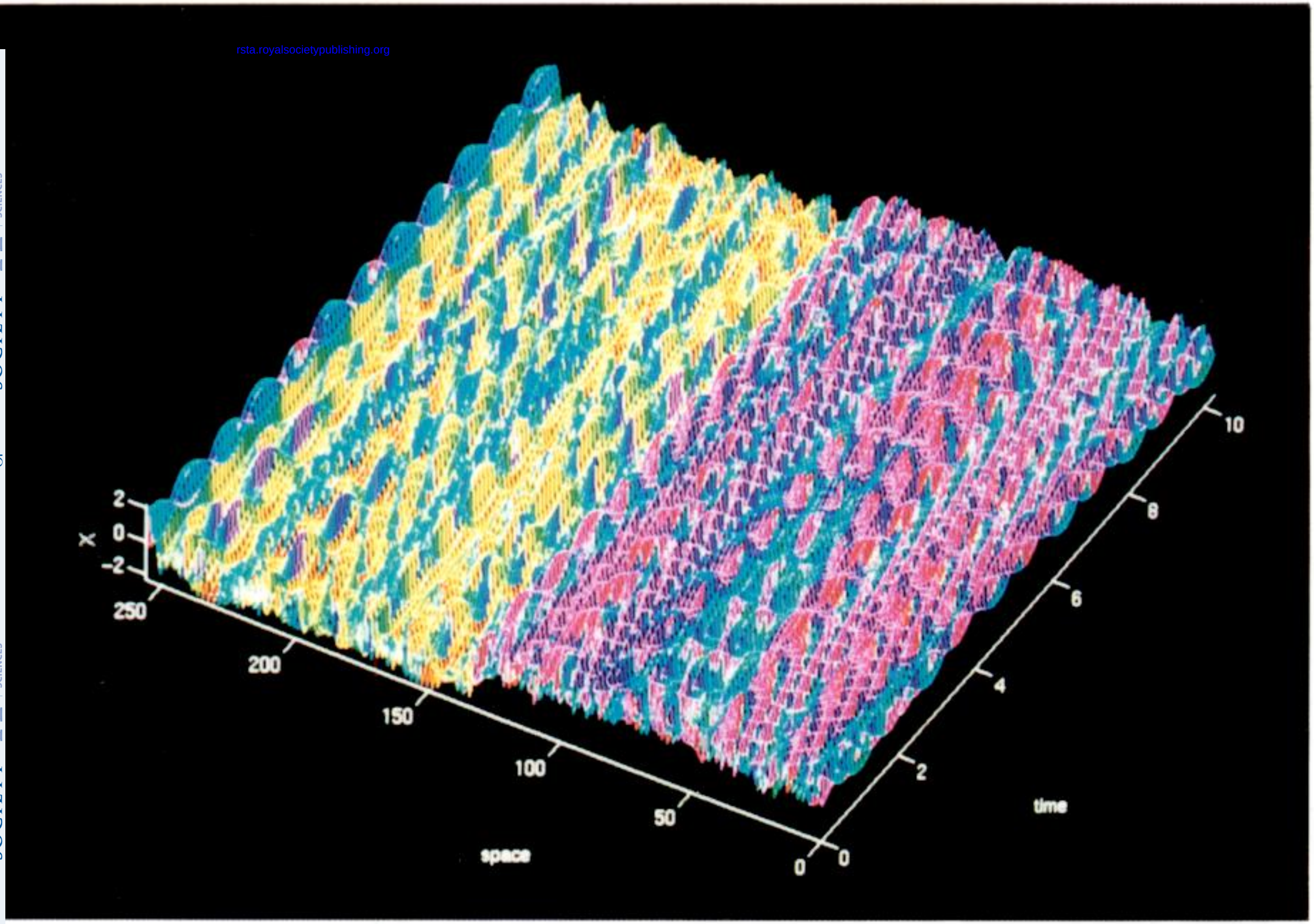

Figure 7. Result corresponding to figure 6 for initial condition (4).

PHILOSOPHICAL TRANSACTIONS OF THE ROYAL SOCIETY A MATHEMATICAL, PHYSICAL & ENGINEERING SCIENCES